



RESEARCH ARTICLE

10.1029/2018JA025788

Pitch Angle Scattering of Energetic Electrons by BBFs

W. W. Eshetu¹ , J. G. Lyon¹ , M. K. Hudson^{1,2}, and M. J. Wiltberger² ¹Department of Physics and Astronomy, Dartmouth College, Hanover, NH, USA, ²High-Altitude Observatory, National Center for Atmospheric Research, Boulder, CO, USA

Key Points:

- Pitch angle scattering of energetic electrons by bursty bulk flow fields in MHD simulations with idealized solar wind input is demonstrated
- A method of calculating the equatorial pitch angle diffusion coefficient for general electromagnetic fields has been developed
- Pitch angle diffusion coefficients are calculated for radiation belt electrons in realistic BBF fields for the first time

Correspondence to:

W. W. Eshetu,
wondwossen.w.eshetu.GR@dartmouth.edu

Citation:

Eshetu, W. W., Lyon, J. G., Hudson, M. K., & Wiltberger, M. (2018). Pitch angle scattering of energetic electrons by BBFs. *Journal of Geophysical Research: Space Physics*, 123, 9265–9274. <https://doi.org/10.1029/2018JA025788>

Received 27 JUN 2018

Accepted 15 OCT 2018

Accepted article online 17 OCT 2018

Published online 16 NOV 2018

Abstract Field line curvature scattering by the magnetic field structure associated with bursty bulk flows (BBFs) has been studied, using simulated output fields from the Lyon-Fedder-Mobarry global magnetohydrodynamic code for specified solar wind input. There are weak magnetic field strength (B) regions adjacent to BBFs observed in the simulations. We show that these regions can cause strong scattering where the first adiabatic invariant changes by several factors within one equatorial crossing of energetic electrons of a few kiloelectron volts when the BBFs are beyond $10 R_E$ geocentric in the tail. Scattering by BBFs decreases as they move toward the Earth or when the electron energy decreases. For radiation belt electrons near or inside geosynchronous orbit we demonstrate that the fields associated with BBFs can cause weak scattering where the fractional change of the first invariant (μ_0) within one equatorial crossing is small, but the change due to several crossings can accumulate. For the weak scattering case we developed a method of calculating the pitch angle diffusion coefficient $D_{\alpha\alpha}$. $D_{\alpha\alpha}$ for radiation belt electrons for one particular BBF were calculated as a function of initial energy, equatorial pitch angle, and radial location. These $D_{\alpha\alpha}$ values were compared to calculated $D_{\alpha\alpha}$ for a dipole field with no electric field. We further compared $D_{\alpha\alpha}$ values with that of stretched magnetic fields calculated by Artemyev et al. (2013, <https://doi.org/10.5194/angeo-31-1485-2013>) at $r \approx 7 R_E$. Results show that scattering by BBFs can be comparable to the most highly stretched magnetic field they studied.

1. Introduction

Observations of the magnetosphere have revealed that the plasma flow in the magnetosphere is highly structured (Angelopoulos et al., 1992; Nakamura et al., 2011; Ohtani et al., 2004; Runov et al., 2009). Angelopoulos et al. (1992) studied high-speed flows in the plasma sheet and used the term bursty bulk flows (BBFs) to characterize the observed flow structures. They showed that BBFs are organized as a burst of flow (>100 km/s) with a 10-min time scale and a peak flow >400 km/s of 1-min time scale. BBFs are believed to be created by localized magnetic reconnection (Chen & Wolf, 1993). They are also believed to represent flux tubes of low entropy, which convect faster than the bulk of the plasma (Pontius & Wolf, 1990). BBFs are associated with many magnetospheric phenomena. BBFs have enhanced B_z , strong induced electric field, and they are associated with dipolarization (Nakamura et al., 2002; Ohtani et al., 2004; Runov et al., 2009). The enhanced B_z is usually preceded with a decrease in B_z and weakened magnetic field strength (Ohtani et al., 2004; Yao et al., 2015; Zhou et al., 2014). BBFs are also interpreted as the equatorial footprint of auroral streamers, a north-south aligned thin auroral arc (Forsyth et al., 2008; Lyons et al., 1999; Nakamura et al., 2001; Sergeev et al., 1999). BBFs are also shown to play a role in accelerating and injecting plasma sheet electrons into the radiation belts (Birn et al., 1998; Gabrielse et al., 2017, 2016; Li et al., 2003; Sarris et al., 2002). Here we study the role of the localized magnetic field structure of the BBFs in the nonadiabatic motion and pitch angle scattering of energetic electrons by the magnetic field structure of BBFs. The quantitative rate of pitch angle scattering is associated with the rate of change of the first adiabatic invariant (Birmingham, 1984; Buchner & Zelenyi, 1989).

The first adiabatic invariant (μ) is conserved in the absence of rapid change in magnetic field on the time and spatial scale of gyromotion and is used to organize transport of energetic particles in the magnetosphere (Schulz & Lanzerotti, 1974). The expression of μ is written as an expansion parameterized by magnetic field inhomogeneity (Northrop, 1963; Young et al., 2002). The leading term in the expansion, $\mu_0 = \frac{p_{\perp}^2}{2 m_0 B}$ is usually used as an approximate invariant. Here m_0 is the particle rest mass, B is the magnitude of the magnetic field, and p_{\perp} is the perpendicular component of the momentum. The conservation of μ_0 can be violated when the fields vary on the time scale of the gyroperiod or when the gyroradius (ρ) is comparable to the gradient scale

length $L = (\frac{|V_B|}{B})^{-1}$, shear length ($\zeta = \frac{B^2}{|\mathbf{B} \cdot \nabla \times \mathbf{B}|}$; Pfefferle et al., 2015; Smets, 2000), or curvature radius (R_c) of the magnetic field. The nonadiabatic motion of charged particles in highly curved magnetic fields has been studied by many authors (Birmingham, 1984; Buchner & Zelenyi, 1989; Chen, 1992; Chirkov, 1978; Engel et al., 2016; Hudson et al., 1997; Sergeev & Tsyganenko, 1982; Speiser, 1991; Ukhorskiy & Sitnov, 2013; Young et al., 2002; Zelenyi et al., 2013).

Speiser (1991) studied the trajectories of particles in the tail current sheet. He showed that the value of the first adiabatic invariant after the particles cross the current sheet is different from the value it had as it approaches the current sheet, which he referred to as a jump in μ . Buchner and Zelenyi (1989) have analyzed the nonadiabatic charged particle motion in two-dimensional tail-like magnetic field reversals. They characterized the motion based on a $\kappa = \sqrt{\frac{R_c}{\rho}}$ parameter. They showed that the particle motion can be chaotic when the κ parameter is the order of unity and can result in pitch angle diffusion. Young et al. (2002) studied the scattering in μ due to field line curvature in a realistic magnetosphere. In their model μ represents the expansion of the first adiabatic invariant (Northrop, 1963) based on the ratio of ρ to curvature radius at the magnetic equator (R_{ceq}). They calculated $\delta\mu$ as a function of $\frac{\rho}{R_c}$ and the variation of R_c along the field line. Young et al. (2008) studied magnetic field induced pitch angle diffusion as a detrapping mechanism in the inner magnetosphere. They calculated a diffusion coefficient for μ based on $\delta\mu$ of Young et al. (2002), and they studied the long-time behavior of particle distributions in the quiet time inner magnetosphere. Hudson et al. (1997) showed field line curvature as a possible detrapping mechanism of transient proton belts. Engel et al. (2016) extended this work to loss of inner zone protons due to field line curvature scattering during strong magnetic storms as the storm time ring current disturbs the magnetic field topology. In this study we show that field line curvature scattering can also result due to the curvature of the field in the weak B region adjacent to BBFs produced using idealized solar wind input to drive a global magnetohydrodynamic (MHD) model of solar wind-magnetosphere interaction (Wiltberger et al., 2015). We demonstrate that μ_0 can change by several times its initial value within one crossing of the equator depending on the energy of the electrons and the location of the BBF. We refer to scattering of this type as strong scattering. For lower energy and as the BBFs move inward the scattering effect weakens. The fractional change of μ_0 with one crossing can be small (<0.1), which we refer to as weak scattering. However, the cumulative effect of several weak scatterings of many crossings can add up. For the weak scattering case we calculate the pitch angle diffusion coefficient ($D_{\alpha\alpha}$) under BBF fields for different initial energy, pitch angle, and at different stages of the BBF propagation. The method used to calculate $D_{\alpha\alpha}$ and the results are described in the subsequent sections. The values of $D_{\alpha\alpha}$ for the dipole field at one radial location for several energies and equatorial pitch angles are calculated for comparison.

2. Chaotic Particle Trajectories in BBFs

To demonstrate chaotic energetic electron trajectories in BBFs, we traced electrons by solving the Lorentz equation using the field output from the Lyon-Fedder-Mobary (LFM) global MHD simulations (Lyon et al., 2004). The Lorentz equation was integrated using volume preserving methods that can be applied to systems with time-dependent electromagnetic fields with good accuracy and conservative properties over long times of simulation (He et al., 2016). The method has been shown to have a long-term fidelity and higher accuracy compared to the traditional Runge-Kutta methods and Boris algorithms. Before delving into the particle tracing we will briefly describe the LFM-MHD simulations to produce BBFs.

2.1. LFM-MHD Simulations of BBFs

The Lyon-Fedder-Mobary (LFM)-MHD simulation that solves the ideal MHD equations on an irregular grid optimized for magnetosphere studies and subject to specified solar wind input (Lyon et al., 2004) was performed to reproduce the observed qualitative features of BBFs using idealized solar wind conditions. The BBFs are believed to be created by bursts of localized magnetic reconnection (Wiltberger et al., 2015). The simulation was done with a high-resolution grid of (212, 256, and 192) in radial, azimuthal, and polar directions, respectively. This corresponds to a grid resolution of about $0.2 R_E$ in the midtail. The resolution is finer closer to and coarser away from the Earth. The LFM-Magnetosphere-Ionosphere Coupler/Solver version of the code which treats the inner boundary at $2 R_E$ as a spherical surface with known conductivity is used (Merkin & Lyon, 2010). The dipole field of the Earth was aligned along the z axis. The LFM x axis points in the direction of the Sun, and the y axis completes the right-hand coordinate system. There is no corotational electric field in this simulation. The solar wind density was set at 5 cm^{-3} , the x component of velocity at -400 km/s . The y and z

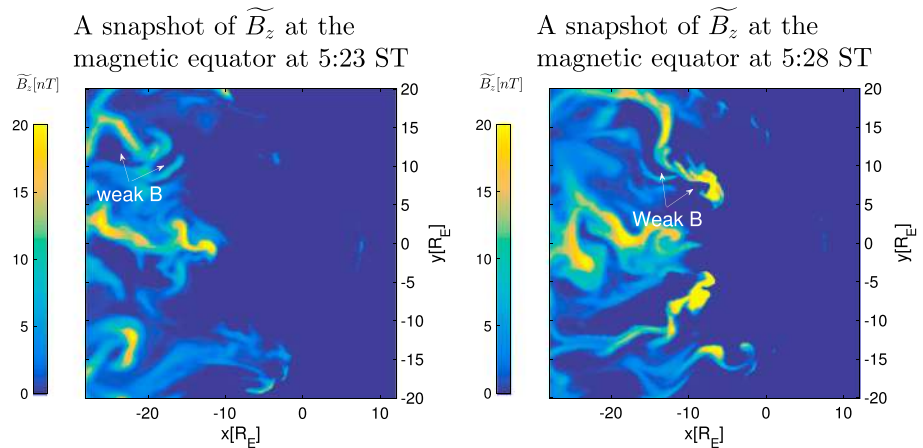


Figure 1. Snapshots of the z component of the perturbed magnetic field, where the z component of the dipole field is subtracted off, (\tilde{B}_z), at the magnetic equator at two different simulation times. The snapshots show an enhanced \tilde{B}_z , which propagates mainly sunward, and adjacent to it are small \tilde{B}_z corresponding to a weak magnetic field region. The weak B region also propagates with the enhanced \tilde{B}_z . A movie showing the evolution of B can be seen in supporting information Movie S2. ST = simulation time.

components of the velocity were set to 0. The density and the velocity were kept fixed throughout the simulations. The x and y components of the interplanetary magnetic field (IMF) were also set to 0. The z component of the IMF is -5 nT for the first 2 hr and flipped to 5 nT for the next 2 hr. Then, after the first 4 hr the IMF was flipped back to -10 nT for the remaining time of the simulations. The LFM fields were dumped at every 1 s of the simulations.

The results of the MHD simulation show earthward propagating BBFs emerging from the magnetotail after about 5 hr of simulation time (ST), 1 hr after the second southward turning of the IMF, which proliferate later. For more detailed characterization of the statistical properties of the flow and the density profile in these BBFs, see the study by Wiltberger et al. (2015). Snapshots of the z component of the perturbed magnetic field (\tilde{B}_z) in the equatorial plane, where the dipole component of the field is subtracted at 5:23 and 5:28 ST are shown in Figure 1. As can be seen from the figure the BBFs have enhanced \tilde{B}_z , but adjacent to these structures, there is also a region of diminished \tilde{B}_z . These regions of diminished \tilde{B}_z also have weak magnetic field strength, and they evolve alongside the enhanced \tilde{B}_z . A movie showing the evolution of \tilde{B}_z and B can be seen in supporting information Movies S1 and S2, respectively. The weak magnetic field (B) regions are found in all the BBF structures of the simulations. This weak field region adjacent to the enhanced \tilde{B}_z moves alongside the BBFs and evolves with the complex structure of the BBFs. The weak field regions are not exclusive to BBFs, but they are different from the other weak B regions as their motion is closely tied to the BBFs. All the BBFs from the

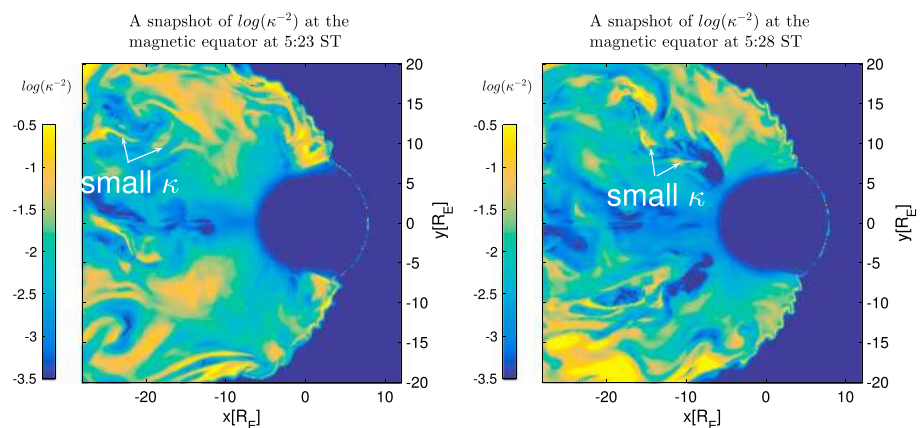


Figure 2. Snapshots of κ^{-2} at the equator corresponding to B_z of Figure 1 showing a small κ in the region of weak B adjacent to the enhanced \tilde{B}_z . ST = simulation time.

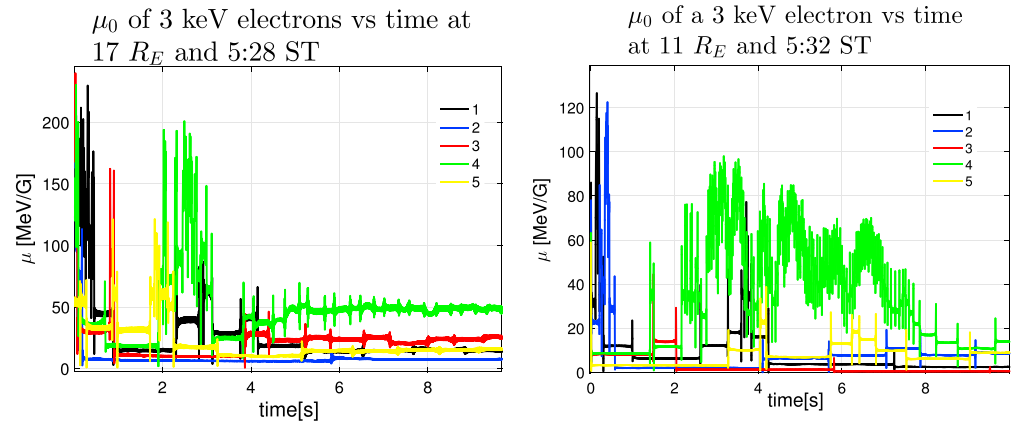


Figure 3. The μ_0 for 3-keV electrons of the same initial pitch angle and randomly chosen gyrophase indicated by different colors, at two radial locations in the chaotic region propagating with the bursty bulk flow near the duskside of the magnetotail in Figure 1. Here $\kappa_{\min} \approx 1.6$ (left) and $\kappa_{\min} \approx 2$ (right). ST = simulation time.

simulations have weak B region flanks; however, the detailed structure differs from one BBF to the other. The detail of the convection within the structure is also complicated, and it is outside the scope of our study. The curvature of the magnetic field in these structures coupled with the weak B can give large $\frac{\rho}{R_c}$, which can cause chaotic motion (Buchner & Zelenyi, 1989; Chen, 1992; Speiser, 1991). Even though the nonadiabatic motion can be caused by small gradient scale length or shear length, we found that the small curvature radius is the main reason for chaotic motion in this case. Snapshots of $\frac{\rho}{R_c} (\kappa^{-2})$, calculated with the gyroradius of a 10 keV and 90° pitch angle electron, corresponding to the snapshots of \tilde{B}_z in Figure 1, are plotted in Figure 2. In order to calculate R_c from MHD fields, we need the derivatives of the components of \tilde{B} . This was done first by calculating the values at the grid positions using center difference method, and the values elsewhere are calculated using linear interpolation in time and all spatial coordinates. The result shows large $\frac{\rho}{R_c}$ adjacent to the BBFs where the magnetic field is weak. Two examples of the weak B regions are marked on the snapshots in Figure 2. We show that this region can cause strong scattering for electrons of energy as low as a few kiloelectron volts.

To demonstrate strong scattering, we traced 3-keV electrons near the BBF coming from the duskside of the magnetotail shown in Figure 1. The electrons were started with a pitch angle of 45° , with randomly chosen gyrophase (different colors in Figure 3 and 4) at the position of $x = -14.7 R_E$ and $y = 9.9 R_E$. For the electrons in this region $\kappa_{\min} \approx 1.6$ for the initial pitch angle. The first adiabatic invariant versus time and the trajectories are shown in Figures 3 and 4. The result shows that μ_0 jumps every time the electrons move through the

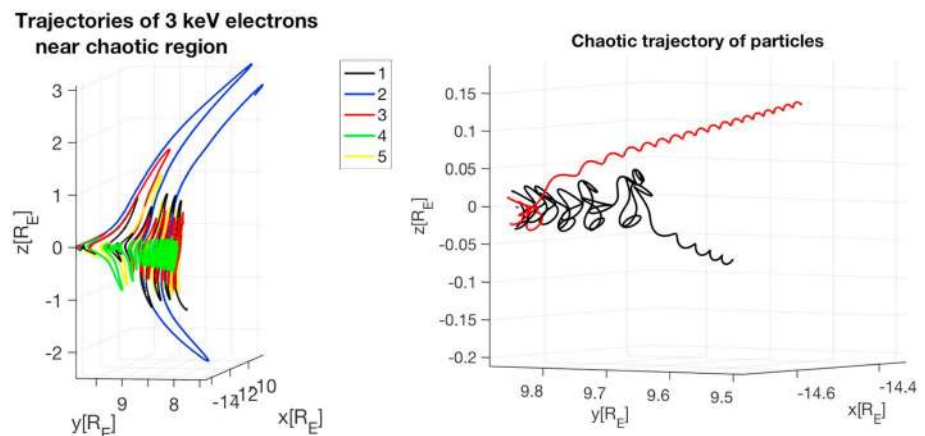


Figure 4. The chaotic trajectories of the 3-keV electrons of randomly chosen initial gyrophase, indicated by different colors, at $17 R_E$ and a zoomed in figure of two of the electrons in the most chaotic region.

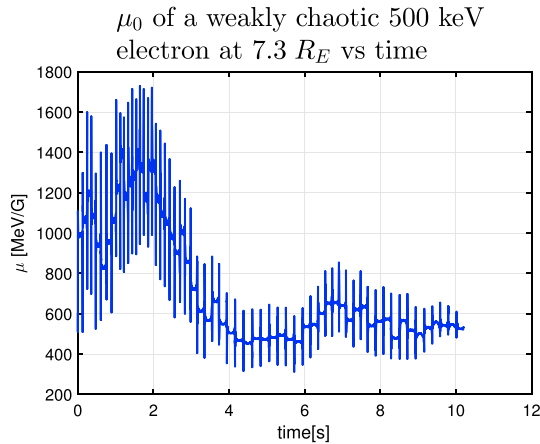


Figure 5. A 500-keV electron in a weakly chaotic region where $\kappa_{\min} \approx 4.5$ showing small $\frac{\delta\mu}{\mu_0}$ but accumulating over several crossings.

magnetic equator, where κ is minimum. The jump of μ_0 ($\delta\mu$) is sensitive and even depends on the gyrophase. It is also random in which the value of $\delta\mu$ every jump is uncorrelated. All are qualitative features of the chaotic trajectories described by Buchner and Zelenyi (1989). A zoomed in figure of the trajectories in the chaotic region shows chaotic trajectories described by Speiser (1991). This chaotic motion is characterized by a strong pitch angle scattering, with a scattering time scale of the bounce motion.

When the BBF moves inward, the weak field around the BBF still moves alongside of the enhanced \tilde{B}_{zr} , as can be seen from Figure 1. However, the $\frac{\rho}{R_c}$ value around the BBF decreases because of the increase of the dipole field strength. Hence, less chaotic particle motion is observed outside the BBF. For this particular BBF, the 3-keV electrons show strong scattering up to $r = 11 R_E$. The μ_0 of the 3-keV electron calculated at $x = -4.0 R_E$, $y = 10.6 R_E$, and $t = 5:32$ ST (simulation time) is shown Figure 3. Even though the $\langle \frac{\delta\mu}{\mu_0} \rangle$ value is smaller than the value calculated at $x = -14.7 R_E$ and $y = 9.9 R_E$, it still corresponds to strong scattering. It should be noted that the 3-KeV electrons at different radial location, used as an example, represent a different population of electrons as they energize while moving inward.

As $\frac{\rho}{R_c}$ decreases, the fractional jumps ($\frac{\delta\mu}{\mu_0}$) will also decrease. However, the jump as a result of several crossings can add up. Since ρ increases with increase of energy, the chaotic region for higher energies penetrates deeper toward Earth. We demonstrate that as the BBF moves inward to the radiation belt region ($< 8 R_E$), radiation belt electrons (> 100 keV) show weakly chaotic motion. We calculate the resulting pitch angle diffusion to estimate the role of deeply penetrating BBFs in pitch angle scattering of radiation belt electrons in the following section.

An example of weakly chaotic behavior in the variation of μ_0 is shown in Figure 5 for electrons of initial energy of 500-keV bouncing through a low κ region (where $\kappa_{\min} \approx 4.5$) near the BBF field located at $x = -3.6 R_E$ and $y = 6.4 R_E$. The result is very similar to the chaotic particle behavior of the strongly chaotic region, except the $\frac{\delta\mu}{\mu_0}$ is much smaller in this case.

We calculate the pitch angle diffusion coefficient ($D_{\alpha\alpha}$) for radiation belt electrons at different radial positions when the BBF penetrates into the radiation belt up to $r = 5.5 R_E$ geocentric for one particular BBF. The method of calculating $D_{\alpha\alpha}$ and the results are presented in the next section.

3. Method of $D_{\alpha\alpha}$ Calculations

The diffusion coefficient was calculated from the ensemble average of $D_{\alpha\alpha} = \langle \frac{\Delta\alpha_{\text{eq}}^2}{2\Delta t} \rangle$, where $\Delta\alpha_{\text{eq}}$ is the difference in the equatorial pitch angle of an electron within time Δt . Δt is chosen to be larger than the bounce period but small compared to the inverse of the calculated diffusion coefficient $\tau = D_{\alpha\alpha}^{-1}$. The ensemble of electrons has the same initial energy and pitch angle and is initiated at the same initial position but with different gyrophase. Since the electrons drift within the simulation period, the result of the $D_{\alpha\alpha}$ is an average around the selected spatial position within a fraction of an Earth radius.

First, the Lorentz trajectories of electrons were calculated with their pitch angle being recorded when they cross the minimum magnetic field location (z_{bmin}). The z_{bmin} is not necessarily at $z = 0$ in the MHD simulations. From now onward, when we say equatorial crossing, we are referring to particles passing through $z = z_{\text{bmin}}$. Then the particle pitch angle (α_0) is transformed to guiding center pitch angle ($\bar{\alpha}$), using the Littlejohn (1983) algorithm. To calculate $\bar{\alpha}$, first, equations (30b) and (30d) of Littlejohn (1983) are used to calculate the parallel (U) and perpendicular (W) velocity of the guiding center. The guiding center pitch angle is then calculated as, $\bar{\alpha} = \tan^{-1}(\frac{W}{U})$. The meaning of the variables used in the formulas can be found in Robert (1981). The modification of the variables for the relativistic case is discussed by Boghosian (2003). The $\bar{\alpha}$ at the equatorial crossing is used in the calculation of $D_{\alpha\alpha}$.

The motivation for using $\bar{\alpha}$ instead of α_0 is as follows. In ensemble averaging of $\frac{\Delta\alpha_{\text{eq}}^2}{2\Delta t}$, there is the assumption that $\Delta\alpha_{\text{eq}}$ is a diffusive change. However, there is also a noncumulative oscillatory change, which oscillates with gyromotion. This oscillation in $\delta\alpha_0$ arises as a result of particles crossing the magnetic equator with different gyrophase as they bounce back and forth. This oscillation does not grow, so it is not diffusive.

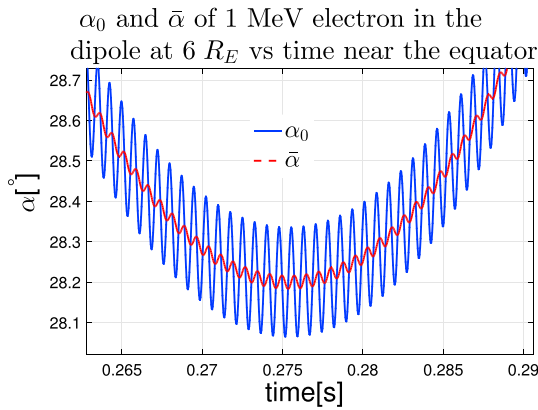


Figure 6. The α_0 and $\bar{\alpha}$ for an electron near the magnetic equator of a dipole field. The α_0 is the local particle pitch angle, and $\bar{\alpha}$ is the guiding center pitch angle defined from the parallel and perpendicular velocities of the guiding center approximated to the order of $\frac{\rho}{L}$ by Littlejohn (1983).

In order to avoid the effect of the noncumulative oscillation in calculation of $D_{\alpha\alpha}$, we use $\bar{\alpha}$. The $\bar{\alpha}$ is free from oscillation in gyrophase up to second order in $\epsilon = \frac{\rho}{L}$ (Littlejohn, 1983). An example of α_0 and $\bar{\alpha}$ versus time for an electron near the equator in a dipole field is shown in Figure 6. The result shows that the oscillations in $\bar{\alpha}$ are much smaller than that of α_0 .

To show how using α_0 overestimates the $D_{\alpha\alpha}$, we compare $D_{\alpha\alpha}$ calculated using $\bar{\alpha}$ and α_0 for electrons of several initial energies and equatorial pitch angles in the Earth's dipole field at $6 R_E$. At each energy and pitch angle an ensemble of 300 electrons with different gyrophase was used. The results are shown in Figure 7. The $D_{\alpha\alpha}$ calculated with α_0 is at least >2 orders of magnitude larger than that of $\bar{\alpha}$ for all initial energies and pitch angles. This is because the $\Delta\alpha_0$ for this electron is dominated by the noncumulative oscillation, whereas in the $\bar{\alpha}$ case there is no oscillation up to ϵ^2 . The ϵ is much less than 1 in this case. The largest value of $D_{\alpha\alpha}$ for a 2-MeV electron calculated using $\bar{\alpha}$ is $\approx 10^{-8.5} \text{ s}^{-1}$ which is equivalent to a diffusion time scale of >10 years. Even this value of $D_{\alpha\alpha}$ has the effect of noncumulative oscillation of the order of ϵ^2 . But the value is so small that the effect has no significance in magnetospheric physics, demonstrating that the method effectively removes the noncumulative oscillation effect in calculating $D_{\alpha\alpha}$.

In the case of strongly chaotic motion where $\frac{\rho}{L}$ and $\frac{\rho}{R_c}$ are not much less than 1, the second-order oscillation in $\bar{\alpha}$ may not be small. However, for weakly chaotic motion we show that the oscillation in the pitch angle ($\bar{\alpha}$) and the first adiabatic invariant ($\bar{\mu}$) due to gyrophase is reasonably small. An example of $\bar{\mu}$ and μ_0 for the weakly chaotic high energy of 500-keV case presented in the previous section is shown in Figure 8. The oscillation in $\bar{\mu}$ in the chaotic region is less than $\delta\mu$. This indicates that the method can be applied for weakly chaotic motion without much error.

In addition, when taking $\Delta\alpha_{eq}$, the electron crossings were chosen to be in the same direction (the same bounce phase), to avoid any oscillatory change in $\bar{\mu}$ due to bounce phase. Furthermore, Δt was also chosen to be several times the bounce period to reduce the effect of second-order oscillations in $\Delta\alpha_{eq}$. Since $\delta\alpha_{eq}$ due to gyromotion does not grow with time, the oscillation term can be reduced by using larger Δt . But Δt must also be much smaller than the diffusive time scale ($D_{\alpha\alpha}^{-1}$) for the diffusion formula to be applicable.

Young et al. (2008) have calculated $D_{\alpha\alpha}$ from $D_{\mu\mu}$ using their empirical model for $\frac{\delta\mu}{\mu}$. In their calculations they use $\mu \propto \sin^2\alpha_{eq}$, which is based on the assumption that the energy is conserved. They also assume that a jump in μ happens within infinitesimal height, and it is constant asymptotically close to the chaotic region. In reality the particles' chaotic motion happens over a finite distance. The finite size of the chaotic region coupled with the presence of electric field in the MHD simulations results in the change of the energy in the chaotic region.

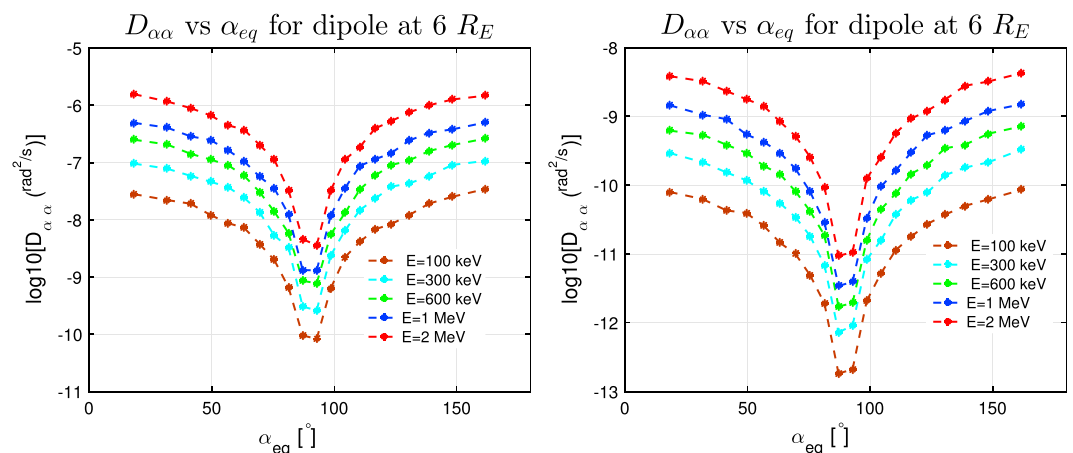


Figure 7. The $D_{\alpha\alpha}$ for energetic electrons at $6 R_E$ in dipole field calculated from particle pitch angle (left) and guiding center pitch angle (right).

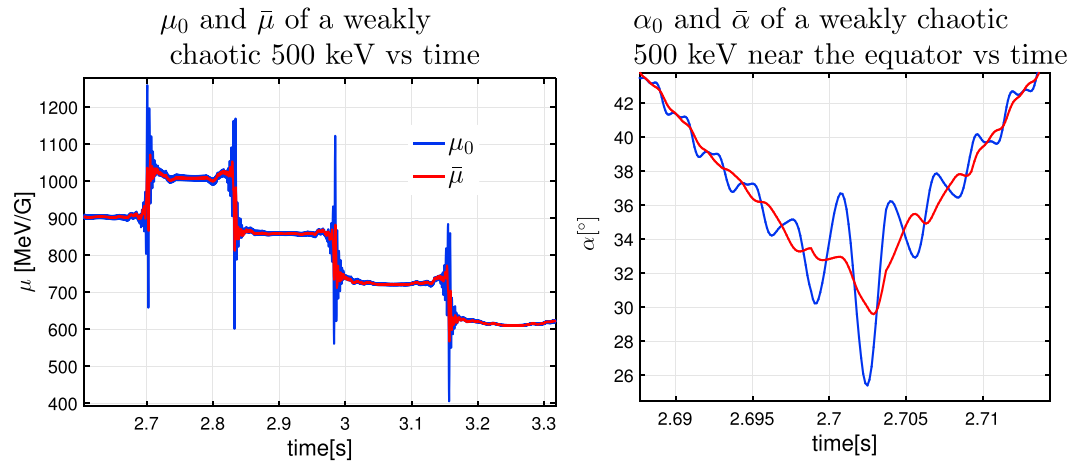


Figure 8. The $\bar{\mu}$ overplotted on μ_0 (left) and $\bar{\alpha}$ overplotted on α_0 (right) as a function of time showing that the guiding center values ($\bar{\mu}$ and $\bar{\alpha}$) averages out the oscillations due to gyrophase.

Thus momentum (p) is not constant. This complicates the calculation of $\delta\alpha_{eq}$ from $\frac{\delta\mu}{\mu_0}$ in the MHD field. Our method does not assume conservation of energy, which makes it appropriate for calculation of $D_{\alpha\alpha}$ for the general electromagnetic case.

4. Results

$D_{\alpha\alpha}$ for radiation belt electrons was calculated near one of the BBFs seen in high-resolution global MHD simulations with prescribed solar wind input (Wiltberger et al., 2015), where the κ parameter is lowest. The results

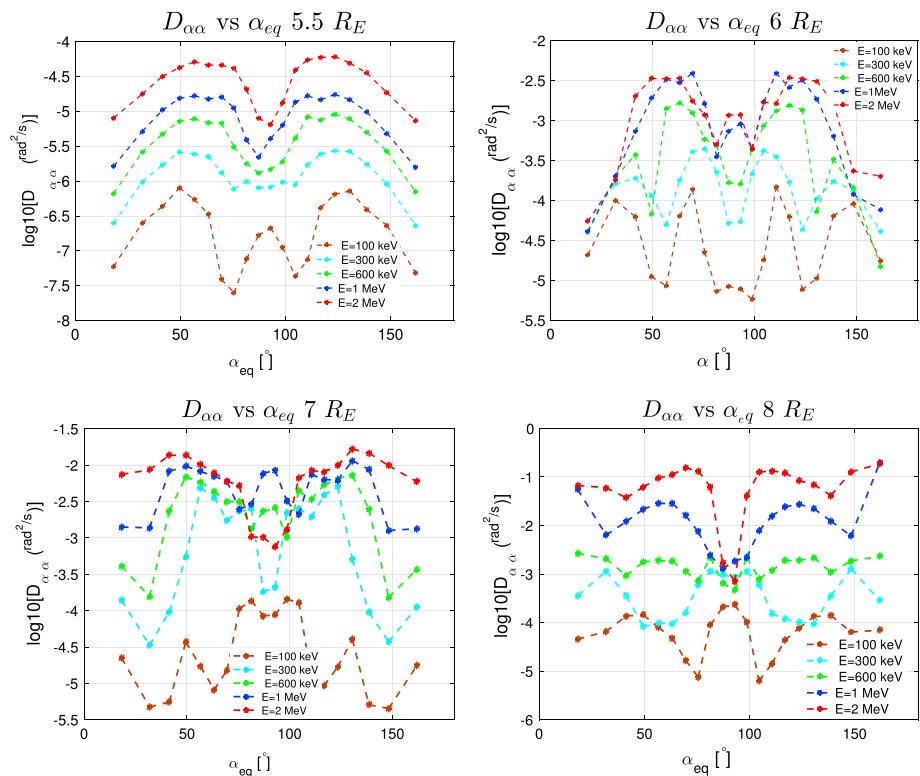


Figure 9. Calculated $D_{\alpha\alpha}$ for different initial energy and equatorial pitch angle at different radial positions of a simulated bursty bulk flow.

of the $D_{\alpha\alpha}$ calculation as a function of initial energy and equatorial pitch angle at different positions of the BBF are shown in Figure 9.

The $D_{\alpha\alpha}$ values with the BBFs is several orders of magnitude larger than that of a dipole field. In general the $D_{\alpha\alpha}$ increases with increase of energy and radial position. This is because the particle motion is more chaotic for larger value of $\frac{\rho}{R_c}$, which happens for higher energy and greater distance from the Earth.

The dependence of $D_{\alpha\alpha}$ on pitch angle can be qualitatively explained as follows. The simulation result shows that, in general for a given energy, $\frac{\delta\mu}{\mu_0}$ is larger for lower α_{eq} . This is true even though ρ is smaller for lower α_{eq} . This results in lower pitch angle particles showing a larger jump in μ_0 and hence in α_{eq} at every equatorial crossing. This result is consistent with the pitch angle dependence of $\frac{\delta\mu}{\mu_0}$ for the field reversal model of Buchner and Zelenyi (1989). However, the bounce time (τ) is larger for lower pitch angle particles, which tends to decrease $D_{\alpha\alpha}$. The dependence $D_{\alpha\alpha}$ on α_{eq} is determined by which of the two effects dominates.

5. Discussion and Conclusions

The simulations presented have demonstrated that energetic electrons, above a few kiloelectron volts, can be scattered by the curvature of the field in the weak B region adjacent to the BBFs seen in global MHD simulations to model BBF observations in the magnetotail (Wiltberger et al., 2015). The weak B regions adjacent to the BBFs are seen in all the BBFs and evolve with the BBFs. However, the morphology and convection in these regions is complicated and has not been well studied. It is not within the scope of this work. Future work should address how this weak B region is related to the BBFs numerically as well as observationally. The simulation results also show that $D_{\alpha\alpha}$ due to pitch angle scattering of the BBFs can be as large as the order of $10^{-2} \frac{\text{rad}^2}{\text{s}}$ for megaelectron volt electrons at $r = 7 R_E$ in the outer radiation belt. Even though the value of $D_{\alpha\alpha}$ is smaller for lower energy and as the BBFs move inward, the pitch angle scattering by BBFs is significant for energetic electrons of >100 keV up to $r = 5.5 R_E$. We compared the results of $D_{\alpha\alpha}$ with that μ scattering in a stretched magnetic field calculated by Artemyev et al. (2013). They have calculated the $D_{\alpha\alpha}$ values for a stretched magnetic field of $B_x = 100 \tanh(\frac{z}{L_c})$ and $B_z = 15$ nT using the Young et al. (2008) method. They choose current sheet thickness (L_c) of 1, 1.5, and 2 R_E . The magnetic field was chosen to approximate the stretched magnetic field at $r \approx 7 R_E$. L_c varies depending on the geomagnetic condition, but the chosen values were realistic values at $r \approx 7 R_E$. Comparing the $D_{\alpha\alpha}$ scattering by the BBF at $r \approx 7 R_E$ with that of Artemyev et al. (2013), the values found from the BBF are about the same order of magnitude as that of $L_c = 1$, which corresponds to the most highly stretched case of the three L_c . For example, for 1-MeV electrons at $\alpha_{\text{eq}} = 45^\circ$, both cases have $D_{\alpha\alpha} \sim 10^{-2} \text{ s}^{-1}$. This indicates that the pitch angle scattering by the BBFs can be equivalent to highly stretched magnetic field line geometry. In addition, Artemyev et al. (2013) have compared the $D_{\alpha\alpha}$ caused by stretched magnetic field and resonant wave—particle scattering by lower band chorus waves. Their result shows that the scattering by stretched field is orders of magnitudes larger for the low pitch angle case; for higher pitch angle electrons the scattering by the chorus wave starts to dominate. For example, for 1 MeV and $L_c = 1 R_E$ the scattering by the stretched field is about 3 orders of magnitude larger than that of chorus waves, and the two are about the same at $\approx 80^\circ$ pitch angle. This indicates that the scattering by BBFs can be dominant mechanism specially at lower pitch angles.

The value of $D_{\alpha\alpha}$ should be interpreted as the maximum value for the particular BBF under study, as it is calculated in the more chaotic region of one particular BBF. However, the qualitative feature of the scattering by the BBF can be generalized to other BBFs with similar magnetic field gradients. In addition, it should be noted that BBFs move with hundreds of kilometer-per-second radial velocity and have spatial structure width the order of 1 R_E (Wiltberger et al., 2015). The scattering by BBFs is a transient phenomenon remaining at a particular position for a time scale of a minute (Angelopoulos et al., 1992). However, the effect of many BBFs can cause significant scattering of radiation belt electrons. The cumulative effect of pitch angle scattering by many BBFs is the topic of future work. The cumulative effect of radial transport and energization by BBFs on plasma sheet electrons injected into the radiation belt region inside geosynchronous orbit is the topic of a separate study (Eshetu et al., 2017).

References

- Angelopoulos, V., Baumjohann, W., Kennel, C. F., Coroniti, F. V., Kivelson, M. G., Pellat, R., et al. (1992). Bursty bulk flows in the inner central plasma sheet. *Journal of Geophysical Research*, *97*, 4027–4039. <https://doi.org/10.1029/91JA02701>
- Artemyev, A. V., Orlova, K. G., Mourenas, D., Agapitov, O. V., & Krasnoselskikh, V. V. (2013). Electron pitch-angle diffusion: resonant scattering by waves vs. nonadiabatic effects. *Annals of Geophysics*, *31*, 1485–1490. <https://doi.org/10.5194/angeo-31-1485-2013>
- Birmingham, T. J. (1984). Pitch angle diffusion in the Jovian magnetodisc. *Journal of Geophysical Research*, *89*, 2699–2707.

Acknowledgments

This work was supported by NASA Grant NNX15AF54G and JHU/APL under 224 NASA contracts NNN16AA09T and NNN06AA01C to UMN and UNH with sub225 contracts to Dartmouth. W. W. Eshetu thanks the NCAR Advanced Study Program for the hospitality in 20016 and Brian Kress for helpful discussion and use of *rbelt3d*. We would like to acknowledge high-performance computing support from Cheyenne provided by NCAR's Computational and Information Systems Laboratory. Simulation results are available via <https://doi.org/10.5281/zenodo.1297605>.

- Birn, J., Thomsen, M. F., Borovsky, J. E., Reeves, G. D., McComas, D. J., Belian, R. D., & Hesse, M. (1998). Substorm electron injections: Geosynchronous observations and test particle simulations. *Journal of Geophysical Research*, *103*(A5), 9235–9248.
- Boghossian, B. (2003). Covariant Lagrangian Methods of Relativistic Plasma Theory, arXiv:physics/0307148v1 [physics.plasm-ph].
- Buchner, J., & Zelenyi, L. M. (1989). Regular and chaotic charged particle motion in magnetotail like field reversals. *Journal of Geophysical Research*, *94*(A9), 11,821–11,842.
- Chen, J. (1992). Nonlinear dynamics of charged particles in the magnetotail. *Journal of Geophysical Research*, *97*(A10), 15,011–15,050.
- Chen, C. X., & Wolf, R. A. (1993). Interpretation of high-speed flows in the plasma sheet. *Journal of Geophysical Research*, *98*(A12), 21,409–21,419.
- Chirkov, B. V. (1978). Problem of charged particle motion stability in a magnetic trap. *Soviet Journal of Plasma Physics*, *4*, 521–541.
- Engel, M. A., Kress, B. T., Hudson, M. K., & Selesnick, R. S. (2016). Comparison of Van Allen Probes radiation belt proton data with test particle simulation for the 17 March 2015 storm. *Journal of Geophysical Research: Space Physics*, *121*, 11,035–11,041. <https://doi.org/10.1002/2016JA023333>
- Eshetu, W., Lyon, J., Wiltberger, M., & Hudson, M. (2017). Test particle simulations of electron injection by the bursty bulk flows (BBFs) using high resolution Lyon-Fedder-Mobarry (LFM) MHD code, 11–15 Dec. New Orleans, LA: Presented at 2017 Fall Meeting, AGU.
- Forsyth, C., Lester, M., Cowley, S. W. H., Dandouras, I., Fazakerley, A. N., Fear, R. C., et al. (2008). Observed tail current systems associated with bursty bulk flows and auroral streamers during a period of multiple substorms. *Annals of Geophysics*, *26*, 167–184.
- Gabrielse, C., Angelopoulos, V., Harris, C., Artemyev, A., Kepko, L., & Runov, A. (2017). Extensive electron transport and energization via multiple, localized dipolarizing bundles. *Journal of Geophysical Research: Space Physics*, *122*, 5059–5076. <https://doi.org/10.1002/2017JA023981>
- Gabrielse, C., Harris, C., Angelopoulos, V., Artemyev, A., & Runov, A. (2016). The role of localized inductive electric fields in electron injections around dipolarizing bundles. *Journal of Geophysical Research: Space Physics*, *121*, 9560–9585. <https://doi.org/10.1002/2016JA023061>
- He, Y., Sun, Y., Zhang, R., Wang, Y., Liu, J., & Qin, H. (2016). High order volume-preserving algorithms for relativistic charged particles in general electromagnetic fields. *Physics of Plasmas*, *23*, 092109. <https://doi.org/10.1063/1.4962677>
- Hudson, M. K., Elkington, S. R., Lyon, J. G., Marchenko, V. A., Roth, I., Temerin, M., et al. (1997). Simulations of radiation belt formation during storm sudden commencements. *Journal of Geophysical Research*, *102*, 14,087–14,102.
- Li, X., Sarris, T. E., Baker, D. N., Peterson, W. K., & Singer, H. J. (2003). Simulation of energetic particle injections associated with a substorm on August 27, 2001. *Geophysical Research Letters*, *30*(1), 1004. <https://doi.org/10.1029/2002GL015967>
- Littlejohn, R. G. (1983). Variational principles of guiding centre motion. *Journal of Plasma Physics*, *29*, 111–125.
- Lyon, J. G., Fedder, J. A., & Mobarry, C. M. (2004). The Lyon-Fedder-Mobarry (LFM) global MHD magnetospheric simulation code. *Journal of Atmospheric and Solar-Terrestrial Physics*, *66*, 1333–1350.
- Lyons, L. R., Nagai, T., Blanchard, G. T., Samson, J. C., Yamamoto, T., Mukai, A., et al. (1999). Association between Geotail plasma flows and auroral poleward boundary intensifications observed by CANOPUS photometers. *Journal of Geophysical Research*, *104*(A3), 4485–4500. <https://doi.org/10.1029/1998JA900140>
- Merkin, V. G., & Lyon, J. G. (2010). Effects of the low-latitude ionospheric boundary condition on the global magnetosphere. *Journal of Geophysical Research*, *115*, A10202. <https://doi.org/10.1029/2010JA015461>
- Nakamura, R., Baumjohann, W., Brittnacher, M., Sergeev, V. A., Kubyshkina, M., Mukai, T., & Liou, K. (2001). Flow bursts and auroral activations: Onset timing and footprint location. *Journal of Geophysical Research*, *106*(A6), 10,777–10,789.
- Nakamura, R., Baumjohann, W., Klecker, B., Bogdanova, Y., Balogh, A., Reme, H., et al. (2002). Motion of the dipolarization front during a flow burst event observed by Cluster. *Journal of Geophysical Research*, *29*(20), 1942. <https://doi.org/10.1029/2002GL015763>
- Nakamura, R., Baumjohann, W., Panov, E., Petrukovich, A. A., Angelopoulos, V., Volwerk, M., et al. (2011). Flux transport, dipolarization, and current sheet evolution during a double-onset substorm. *Journal of Geophysical Research*, *116*, A00136. <https://doi.org/10.1029/2010JA015865>
- Northrop, T. G. (1963). *The adiabatic motion of charged particles*. New York: Intersci. Publ.
- Ohtani, S., Shay, M. A., & Mukai, T. (2004). Temporal structure of the fast convective flow in the plasma sheet: Comparison between observations and two-fluid simulations. *Journal of Geophysical Research*, *109*, A03210. <https://doi.org/10.1029/2003JA010002>
- Pfefferle, D., Graves, J. P., & Cooper, W. A. (2015). Hybrid guiding-centre/full-orbit simulations in non-axisymmetric magnetic geometry exploiting general criterion for guiding-centre accuracy. *Plasma Physics and Controlled Fusion*, *57*, 054017. <https://doi.org/10.1088/0741-3335/57/5/054017>
- Pontius, D. H., & Wolf, R. A. (1990). Transient flux tubes in the terrestrial magnetosphere. *Geophysical Research Letters*, *17*, 49–52.
- Robert, G. L. (1981). Hamiltonian formulation of guiding center motion. *The Physics of Fluids*, *24*, 1730. <https://doi.org/10.1063/1.863594>
- Runov, A., Angelopoulos, V., Sitnov, M. I., Sergeev, V. A., Bonnell, J., McFadden, J. P., et al. (2009). THEMIS observations of an earthward propagating dipolarization front. *Geophysical Research Letters*, *36*, L14106. <https://doi.org/10.1029/2009GL038980>
- Sarris, T. E., Li, X., Tsaggas, N., & Paschalidis, N. (2002). Modeling energetic particle injections in dynamic pulse fields with varying propagation speeds. *Journal of Geophysical Research*, *107*(A3), 1033. <https://doi.org/10.1029/2001JA900166>
- Schulz, M., & Lanzerotti, L. J. (1974). *Particle diffusion in the radiation belts*. Berlin: Springer.
- Sergeev, V. A., Liou, K., Meng, C.-I., Newell, P. T., Brittnacher, M., Parks, G., & Reeves, G. D. (1999). Development of auroral streamers in association with localized impulsive injections to the inner magnetotail. *Journal of Geophysical Research*, *26*, 417–420.
- Sergeev, V. A., & Tsyganenko, N. A. (1982). Energetic particle losses and trapping boundaries as deduced from calculations with a realistic magnetic field model. *Planetary and Space Science*, *30*(10), 999–1006. [https://doi.org/10.1016/0032-0633\(82\)90149-0](https://doi.org/10.1016/0032-0633(82)90149-0)
- Smets, R. (2000). Charged particle dynamics in tangential discontinuity. *Journal of Geophysical Research*, *105*(A11), 25,009–25,020.
- Speiser, T. W. (1991). Particle motion in the tail current sheet. *Advances in Space Research*, *11*(9), 151–159.
- Ukhorskiy, A. Y., & Sitnov, M. I. (2013). Dynamics of radiation belt particles. *Space Science Reviews*, *179*, 545–578. <https://doi.org/10.1007/s11214-012-9938-5>
- Wiltberger, M., Merkin, V., Lyon, J. G., & Ohtani, S. (2015). High-resolution global magnetohydrodynamic simulation of bursty bulk flows. *Journal of Geophysical Research: Space Physics*, *120*, 4555–4566. <https://doi.org/10.1002/2015JA021080>
- Yao, Z. H., Liu, J., Owen, C. J., Forsyth, C., Rae, I. J., Pu, Z. Y., et al. (2015). A physical explanation for the magnetic decrease ahead of dipolarization fronts. *Annals of Geophysics*, *33*, 1301–1309. <https://doi.org/10.5194/angeo-33-1301-2015>
- Young, S. L., Denton, R. E., Anderson, B. J., & Hudson, M. K. (2002). Empirical model for μ scattering caused by field line curvature in a realistic magnetosphere. *Journal of Geophysical Research*, *107*(A6), 1069. <https://doi.org/10.1029/2000JA000294>

- Young, S. L., Denton, R. E., Anderson, B. J., & Hudson, M. K. (2008). Magnetic field line curvature induced pitch angle diffusion in the inner magnetosphere. *Journal of Geophysical Research*, *113*, A03210. <https://doi.org/10.1029/2006JA012133>
- Zelenyi, L. M., Neishtadt, A. I., Artemyev, A. V., Vainchtein, D. L., & Malova, H. V. (2013). Quasiadiabatic dynamics of charged particles in a space plasma. *Physics-Uspeski*, *56*, 347–394. <https://doi.org/10.3367/UFNe.0183.201304b.0365>
- Zhou, X.-Z., Angelopoulos, V., Liu, J., Runov, A., & Li, S.-S. (2014). On the origin of pressure and magnetic perturbations ahead of dipolarization fronts. *Journal of Geophysical Research: Space Physics*, *119*, 211–220. <https://doi.org/10.1002/2013JA019394>